Novel Evaluation Method for Leakage Electromagnetic Field Using Coil Scaling Law for Wireless Power Transfer System for Battery Electric Vehicle *

Hayato SUMIYA Eisuke TAKAHASHI Nobuhisa YAMAGUCHI
Keisuke TANI Sakahisa NAGAI Toshiyuki FUJITA
Hiroshi FUJIMOTO

特集

A wireless power transfer system for battery electric vehicles needs to be evaluated in its leakage electromagnetic field (EMF). It is determined to be measured at 10 m point when the maximum power is transmitted between full-scale coils. In this paper, we propose a novel evaluation method for EMF using coil scaling law. Using coil scaling law, we can simplify and increase measuring speed to verify satisfying the EMF regulation. The satisfying conditions which enable equivalent evaluation between full-scale coils and mini-scale ones are derived.

Key words :
Battery electric vehicle, Wireless power transfer, EMC

1. Introduction

In order to prevent global warming, reducing CO_2 emissions is an effective method [1]. To achieve it, the electrification of automobiles needs to progress. However, battery electric vehicles (BEV) have some disadvantages against internal combustion engine vehicles. The most crucial issue is the mileage per charge.

To improve the above problem, wireless power transfer (WPT) systems are studied to charge BEV in stationary and in dynamic [2-5]. This system is advantageous and useful to promote BEV. However, in order to sell WPT systems, evaluation of EMF and electromagnetic compatibility (EMC) are necessary. These are defined as the standardization in 6) and 7). In general, the EMF and EMC are measured using full-sized equipment which include not only measuring instruments, but also power equipment such as power supplies, coil pairs (long wires and large

＊（一社）自動車技術会の了承を得て，EVTeC2021, No. 20214354, Yokohama, Japan, 2021 より一部加筆して転載

ferrite cores). Moreover, a full-scaled coil is very big and high cost since WPT needs high power transfer. In development period, repeated evaluations are undesirable to satisfy the regulations.

We have proposed the coil scaling law to simplify the EMF and the EMC measurements in 8) and 9). Using coil scaling law, we can simplify and increase measuring speed to verify satisfying the EMF and the EMC regulation in a development period. Three satisfying conditions are derived from theoretical calculations and circuit topology. The effectiveness of the proposal is confirmed by experiments. However, these are considered AC output and are considered only the basic order component of the EMF and the EMC. In this paper, we propose the novel evaluation method using coil scaling law considering the harmonic order components. we show the effectiveness that harmonic components are as effective as fundamental components from the simulations and the experiments.

2. SS circuit topology

In this section, series-series circuit topology using in the WPT, as shown in Fig. 1 is explained [8) 9)]. The primary current I_p and secondary current I_s are represented by

$$I_p = \frac{(r_s + R_L)}{(\omega M_p s)^2 + r_p (r_s + R_L)} V_p, \tag{1}$$

$$I_s = -\frac{j\omega M_{ps}}{(\omega M_{ps})^2 + r_p(r_s + R_L)} V_p, \tag{2}$$

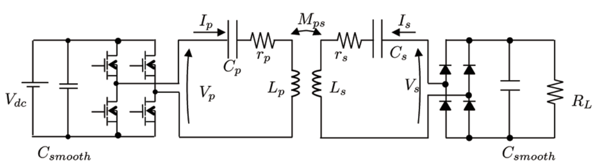

Fig. 1 SS circuit topology

where r_p and r_s are the primary and secondary coil resistance, ω is the resonance angular frequency, M_{ps} is the mutual inductance between the primary and secondary coils, R_L is the load resistance, and V_p is the input AC voltage, respectively. Coupling coefficient k, optimum load resistance R_{Lopt}, and maximum coil efficiency when the load is the optimum coil resistance are calculated as

$$k = \frac{M_{ps}}{\sqrt{(L_p L_s)}}, \tag{3}$$

$$R_{Lopt} = \sqrt{r_s^2 + \frac{r_s(\omega M_{ps})^2}{r_p}}, \tag{4}$$

$$\eta_{max} = \frac{k^2 Q_p Q_s}{\left(1 + \sqrt{(1 + k^2 Q_p Q_s)}\right)^2} \tag{5}$$

where L_p and L_s are primary and secondary self-inductances, Q_p and Q_s are Q factor defined by $Q=\omega L/R$, respectively.

3. Satisfying conditions

In this section, we describe satisfying conditions to evaluate the EMF and the EMC using the scaling law [8)].

3.1 Parameter scaling in mini-scale coil

In this paper, the coil scaling ratio is defined as α, and we assume that the longitudinal, lateral, and vertical scaling ratios are the same. In these conditions, the mini-scale coil parameters are described as

$$L_i' = \frac{1}{\alpha} L_i, \tag{6}$$

$$M_{ps}' = \frac{1}{\alpha} M_{ps}, \tag{7}$$

$$r_i' = \alpha r_i, \tag{8}$$

where superscript′ indicate scaling model, and subscript i indicate p or s respectively (8). Using equations (6)-(8), Q factor and coupling coefficient in the scale model are represented by

$$Q_i' = \frac{1}{\alpha^2}\frac{\omega'}{\omega}Q_i, \tag{9}$$

$$k' = \frac{M_{ps}'}{\sqrt{(L_p' L_s')}} = k. \tag{10}$$

From these equations are indicated that we can use the resonance angular frequency as a parameter to derive the satisfied condition measuring equivalent evaluation between the full-scale coils and the mini-scale ones. Moreover, these indicate that the coupling coefficients between the full-scale coils and the mini-scale ones are the same. Finally, maximum efficiency of the mini scale coils is given by

$$\eta_{max}' = \frac{k^{2\prime} Q_p' Q_s'}{\left(1+\sqrt{(1+k^{2\prime} Q_p' Q_s')}\right)^2}. \tag{11}$$

3.2 Same efficiency conditions

The same efficiency condition between the full-scale coils and the mini-scale ones is important. From (5) and (11), the kQ product should be the same to satisfy the condition. The full-scale coil coupling coefficient and the mini-scale coil ones are the same. Therefore, equalizing the full-scale Q factor and the mini-scale Q factor is suitable in this paper. Finally, the following relation holds, it is necessary that the below equation is satisfied.

$$\omega' = \alpha^2 \omega \tag{12}$$

In this condition, the primary current Ip' and the secondary current Is' in the mini-scale coils are represented by

$$I_p' = \frac{1}{\alpha}\frac{r_s + R_L}{(\omega M_{ps})^2 + r_p(r_s + R_L)}V_p', \tag{13}$$

$$I_s' = -\frac{1}{\alpha}\frac{\omega M_{ps}}{(\omega M_{ps})^2 + r_1(r_s + R_L)}V_p. \tag{14}$$

3.3 Same magnetic flux density condition

In the same efficiency condition between the full-scale coils and the mini-scale coils, we derive the condition that is the same magnetic flux density. Magnetic flux density on the coil is expressed by the following equation.

$$B_i = \frac{L_i I_i}{a_i b_i} \tag{15}$$

Here, Bi is the full-scale coil magnetic flux density, ai and bi are the coil size parameter. In the mini-scale coil, below equations are satisfied.

$$B'_i = \frac{L_i' I_i'}{a_i' b'} = \alpha \frac{L_i I_i'}{a_i b_i} \tag{16}$$

Here, *B'i* is the mini-scale coil magnetic flux density, and ai' and bi' are mini-scale coil size parameters. In order to achieve the same magnetic flux density between the full-scale coils and the mini-scale ones, they must be equal. In fact, the following equation is derived from (15) and (16).

$$I_i' = \frac{1}{\alpha}I_i \tag{17}$$

Based on (1), (2), (15), and (16), the condition which satisfies (17) is derived as

$$V_p' = V_p. \tag{18}$$

This is one of the satisfying conditions that achieves the same magnetic flux density. In this condition, transfer power is given as the following equation.

$$P_{out}' = \frac{1}{\alpha}P_{out} \tag{19}$$

特集

3.4 Satisfying conditions

Summarizing above, three satisfying conditions are derived from circuit topology and theoretical calculations. First, the longitudinal, lateral, and vertical scaling ratios are the same. These are satisfying with the same coupling coefficient between the full-scale coils and the mini-scale coils. Second, the mini-scale coils resonant frequency is set as (12). And the last, the voltage input in the full-scale coils and the mini-scale ones is set as the same. When these three conditions are satisfied, there is no change in coupling coefficient, efficiency, and magnetic flux density. In fact, we can equivalently evaluate the efficiency, magnetic flux density and the EMF of the full-scale coils using the mini-scale coils.

4. Simulation results

In order to confirm the scaling law, we conduct simulations using SS circuit topology, as shown in Fig. 1. In this paper, the scaling ratio α is set to α=4. Table 1 shows the coil specifications and Fig. 2 shows the full-scale coils and Fig. 3 shows the mini-scale coils. Table 2 shows the coil parameters, which are measured by an LCR meter. The full-scale coils are used 85 kHz and the mini-scale coils are used 1360 kHz, which is derived from (12). The self-inductance and the mutual inductance are slightly higher than the theoretical values since we use the same thickness ferrite cores between the full-scale coils and the mini-scale ones due to availability issues. r_{pDC} and r_{sDC} are the DC coil resistance, and r_{pf} and r_{sf} are the AC coil resistance measured at resonance frequencies, respectively. The DC coil resistances are larger than theoretical values because the number of strands of mini-scale coil is reduced due to the assembly problem.

In addition, the secondary resistance is higher than the primary resistance. This coil is designed as an in-vehicle coil so that this reduces the coil size. For these reasons, the efficiency of mini-scale coil is slightly smaller than the full-scale one. The full-scale and the mini-scale voltage inputs are the same, and the primary current, the secondary current, and the power are following the scaling law as shown in Fig. 4 ~ Fig. 7 and Table 3. Fig. 8 and Fig. 9 show the EMF and the EMC. These are calculated by the finite element method

Table 2 Coil parameters

Item	Full-scale	Mini-scale	Ratio(Theoretical value)
$L_p[\mu H]$	241.9	64.0	0.265(0.25)
$L_s[\mu H]$	96.5	25.3	0.262(0.25)
$M[\mu H]$	13.7	3.6	0.263(0.25)
$k[-]$	0.089	0.089	1.0(1.0)
$f[kHz]$	85	1360	16.0(16.0)
$r_{pDC}[m\Omega]$	46.5	369.0	7.9(4.0)
$r_{sDC}[m\Omega]$	15.8	131.0	8.3(4.0)
$R_L[m\Omega]$	4.3	18.2	4.0(4.0)
$r_{pf}[m\Omega]$	122.5	488.0	4.0(4.0)
$r_{sf}[m\Omega]$	41.8	794.0	19.0(4.0)
Q_p	1051.9	1122.1	1.1(1.0)
Q_s	1232.4	273.3	0.2(1.0)
η	0.981	0.960	2.1pt.(0pt.)

Table 3 Simulation results

Item	Full model	Mini model	Ratio (Theoritical value)
V_{in} [V]	200	200	1 (1)
f [kHz]	85	1360	16 (16)
I_p [Arms]	14.0	3.6	0.259 (0.25)
I_s [Arms]	23.7	5.7	0.242 (0.25)
P [kW]	2.4	0.6	0.25 (0.25)
η [-]	0.967	0.938	-2.9pt (0)

Table 1 Comparison of coil specifications (Full-scale and Mini-scale)

Item	Full-scale	Mini-scale
Primary coil size [mm]	$1000 \times 250(t=5)$	$250 \times 62.5(t=1.25)$
Secondary coil size [mm]	$185 \times 185(t=5)$	$46.25 \times 46.25(t=1.25)$
Primary core size [mm]	$1026 \times 294(t=5)$	$256.4 \times 73.5(t=5)$
Secondary core size [mm]	$200 \times 200(t=5)$	$50 \times 50(t=5)$
Goil gap between primary coil and secondary coil [mm]	$z=100$	$z=25$
Clearance between primary coil and core [mm]	2.0	0.5
Clearance between Secondary coil and core [mm]	2.0	0.5
Clearance between coil and case [mm]	0.2	0.2
Litz wire	Strand: 0.05mm, Number: 6250	Strand: 0.05mm, Number;200

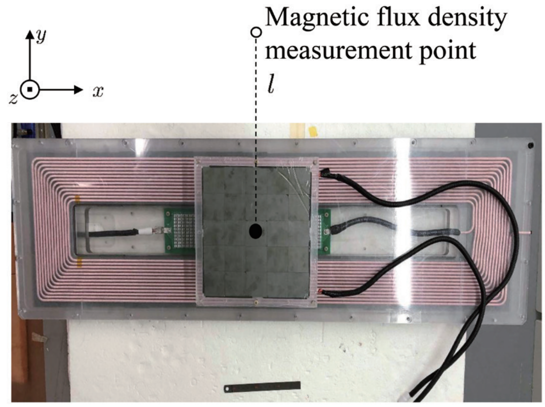

Fig. 2　Full-scale coils

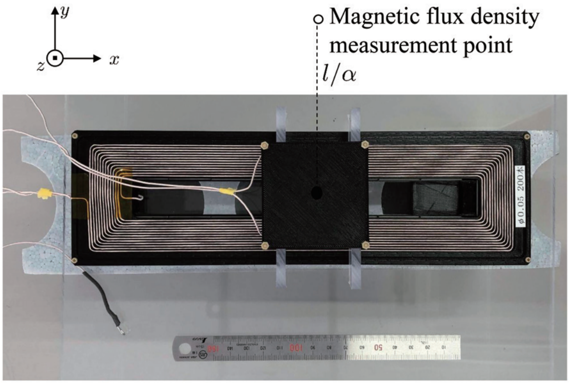

Fig. 3　Mini-scale coils

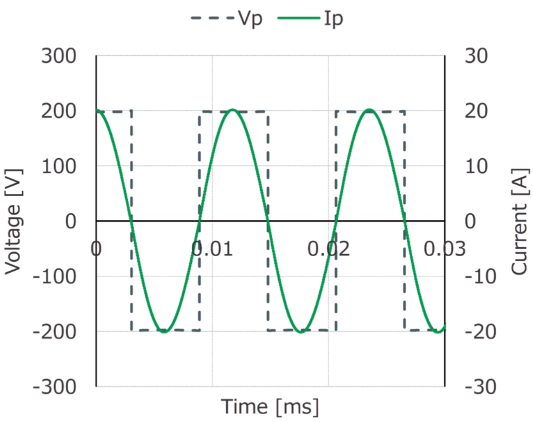

Fig. 4　Simulation results (full scale model Vp, Ip)

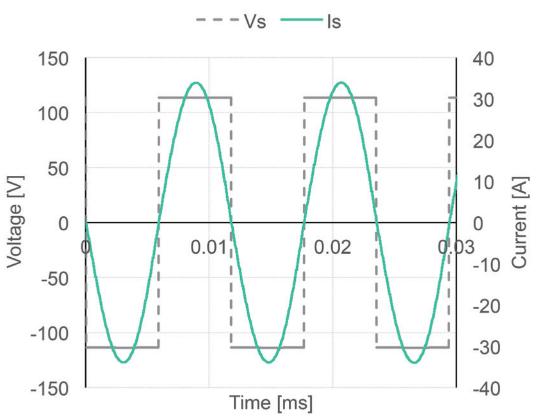

Fig. 5　Simulation results (full scale model Vs, Is)

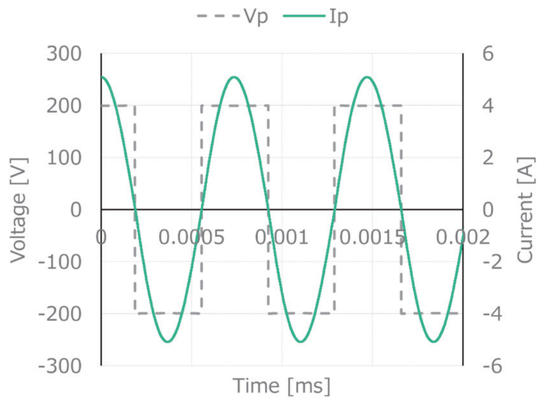

Fig. 6　Simulation results (mini scale Vp, Ip)

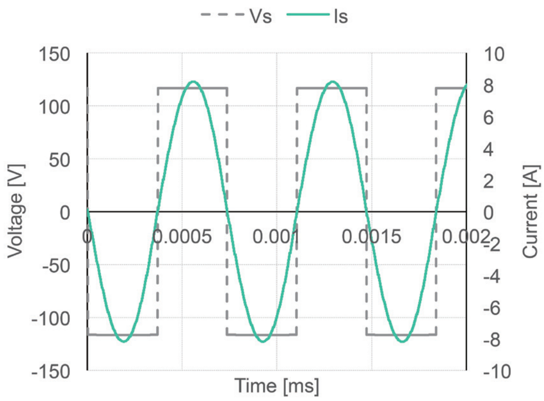

Fig. 7　Simulation results (mini scale Vs, Is)

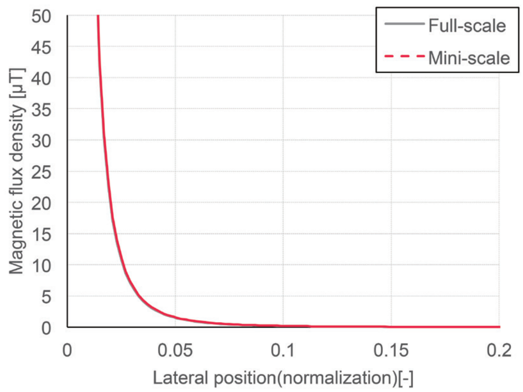

Fig. 8　Simulation results of EMF

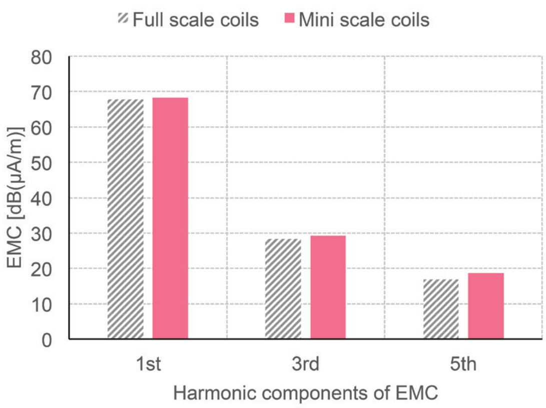

Fig. 9　Simulation results of EMC

and using the primary and the secondary currents calculated by the circuit simulations. EMF is simulated the magnetic flux density from the coil center position to the lateral directions as shown in Fig. 2 and Fig. 3. These situational points are followed the scaling law so that the full-scale model calculated distance is set to 10 m and the mini scale model calculated distance is set to 2.5m. Moreover, these results are normalized. The EMF generated by the full-scale model and the mini-scale model are the almost same from Fig. 8. The EMC of the full-scale coils is calculated at (x, y, z) = (0m, 10m, 1m) and the EMC of the mini-scale coils is calculated at (x, y, z) = (0m, 2.5m, 0.25m). These simulation conditions are followed as the scaling law. The EMCs are almost the same not only in basic order but also 3rd and 5th harmonic order components as shown in Fig. 9. From these results. the effectiveness of the scaling raw is verified.

5. Experimental results

In this section, the effectiveness of scaling law is confirmed by experimental results. In experiments, a SiC inverter is used in the full-scale experiment, while a GaN inverter is used in the mini-scale experiment. Table 4 and Fig. 10 ~ Fig. 14, show the experimental results. In the experiment, the voltages of the full-scale coils and the mini-scale coils are different since there are resonance frequency errors from the theoretical frequency by the parasitic capacitance of the wiring. The voltages are adjusted that each current become the same. The EMF of the full-scale coils is measured at (x, y, z) = (0, 500 mm, 100mm). The EMF of the mini-scale coils is measured at (x, y, z) = (0, 125mm, 25mm). This point is a 1/4 point on the full-scale one. The EMFs are the almost same between the full-scale coils and the mini-scale ones. From these results, the effectiveness of scaling law to evaluate the EMF is confirmed by experimental results.

Table 4 Experimental results

Item	Full model	Mini model	Ratio (Theoritical value)
V_{in} [V]	40	35	1 (1)
f [kHz]	85	1360	16 (16)
I_p [Arms]	3.1	0.73	0.235 (0.25)
I_s [Arms]	4.6	0.76	0.170 (0.25)

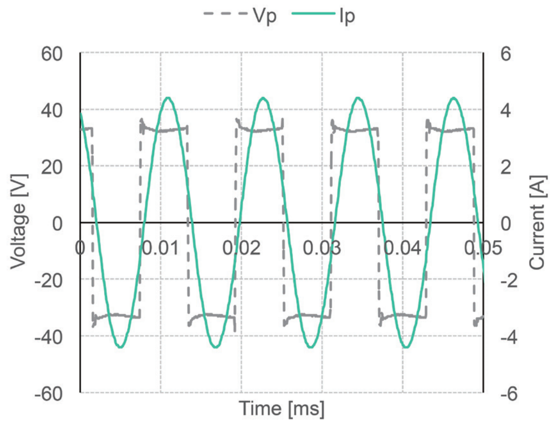

Fig. 10 Experimental results (full scale Vp. Ip)

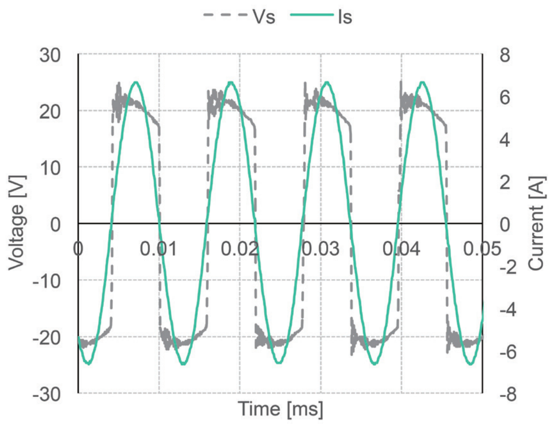

Fig. 11 Experimental results (full scale Vs, Is)

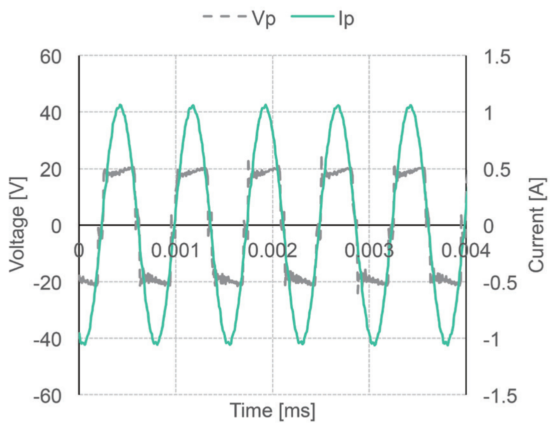

Fig. 12 Experimental results (minis scale Vp, Ip)

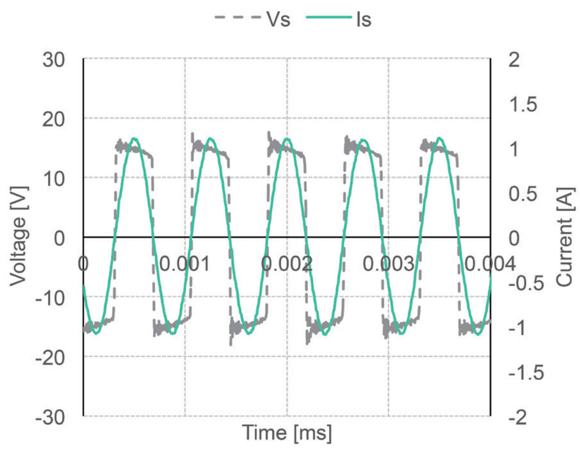

Fig. 13 Experimental results (minis scale Vp, Ip)

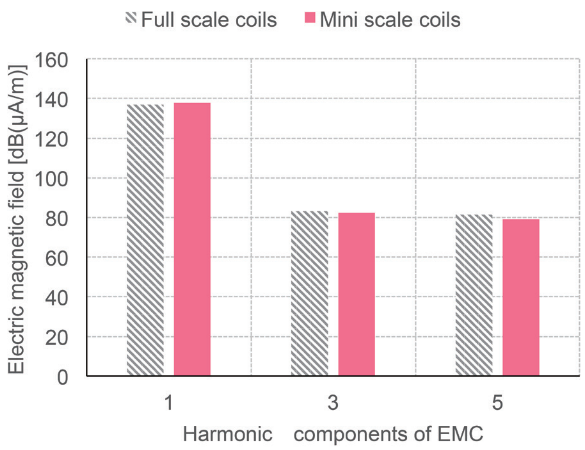

Fig. 14 Experimental results of EMF

6. Conclusion

In this paper, we proposed the novel evaluation method for EMF using the coil scaling law and confirmed its effectiveness by the simulation and the experimental results. Moreover, the scaling law is able to measure not only the basic component but also the harmonic components.

7. Acknowledgment

This work was partly supported by JST-Mirai Program Grant Number JPMJMI21E2, Japan.

References

1) United States Environmental Protection Agency: "Data on Cars used for Testing Fuel Economy"

2) Andre Kurs, Aristeidis Karalis, Robert Moffatt, J.D. Joannopoulos, Peter Fisher, and Marin Soljacic: "Wireless power transfer via strongly coupled magnetic resonances", Sciences, Vol. 317, No. 5834, p. 83(4), 2007

3) Hiroshi Fujimoto, Osamu Shimizu, Sakahisa Nagai, Toshiyuki Fujita, Daisuke Gunji, and Yoichi Ohmori: "Development of Wireless In-wheel Motors for Dynamic Charging from 2nd to 3rd generation", IEEE PELS workshop on Emerging Technologies Wireless Power, Korea, 2020(to be presented).

4) G Coquery, Virginie Deniau, and Alexandre De Bernardinis:"Dynamic Wireless Power Transfer Charging Infrastructure for Future EVs From Experimental Track to Real Circulated Roads Demonstrations", World Electric Vehicle Journal, Vol. 10, No. 84, pp. 1–22, 2019.

5) Osamu Shimizu, Sakahisa Nagai, Toshiyuki Fujita, and Hiroshi Fujimoto:" Potential for CO_2 Reduction by Dynamic Wireless Power Transfer for Passenger Vehicles in Japan", Energies, Vol. 13, No. 13, p. 3342, Jun 2020.

6) SAE. "SURFACE VEHICLE RECOMMENDED PRACTICE", Society of Automotive Engineers, 2016.

7) IEC."Electric vehicle wireless power transfer (WPT) systems - Part 1 General requirements", 2015

8) Hayato Sumiya, Eisuke Takahashi, Nobuhisa Yamaguchi, Keisuke Tani, Toshiyuki Fujita, and Hiroshi Fujimoto, "Proposal of Electromagnetic Field Measurement Method Considering Coil Scaling Ratio of Wireless Power Transfer System for Electric Vehicle" 2020 JSAE Annual Congress(Autumn), 2020

9) Hayato Sumiya, Eisuke Takahashi, Nobuhisa Yamaguchi, Keisuke Tani, Sakahisa Nagai, Toshiyuki Fujita, and Hiroshi Fujimoto, "Coil Scaling Law of Wireless Power Transfer Systems for Electromagnetic Field Leakage Evaluation for Electric Vehicles" IEEJ Transactions on Industry Applications, Vol. 141, No.3, pp.283-292, 2021

特集

著者

角谷 勇人
すみや はやと

エレクトリフィケーションシステム開発部
非接触給電，走行中給電の開発に従事

高橋 英介
たかはし えいすけ

エレクトリフィケーションシステム開発部
非接触給電，走行中給電の開発に従事

山口 宜久
やまぐち のぶひさ

エレクトリフィケーションシステム開発部
非接触給電，走行中給電の開発に従事

谷 恵亮
たに けいすけ

エレクトリフィケーションシステム開発部
非接触給電，走行中給電の開発に従事

永井 栄寿
ながい さかひさ

東京大学大学院新領域創成科学研究科
特任助教　博士（工学）
非接触給電，走行中給電の研究に従事

藤田 稔之
ふじた としゆき

東京大学大学院新領域創成科学研究科
特任講師　博士（工学）
非接触給電，走行中給電の研究に従事

藤本 博志
ふじもと ひろし

東京大学大学院新領域創成科学研究科
教授　博士（工学）
走行中給電，電動車両の運動制御，モータ制御の研究に従事